47th AIAA/ASME/ASCE/AHS/ASC Structures, Structural Dynamics, and Materials Confere
1 - 4 May 2006, Newport, Rhode Island

AIAA 2006-1683

Analysis of the Lenticular Jointed MARSIS Antenna Deployment

Mehran Mobrem*
NGST Astro Aerospace, Carpinteria, CA, 93013

and

Douglas S. Adams†
Jet Propulsion Laboratory, California Institute of Technology, Pasadena, CA, 91109

This paper summarizes important milestones in a yearlong comprehensive effort which culminated in successful deployments of the MARSIS antenna booms in May and June of 2005. Experimentally measured straight section and hinge properties are incorporated into specialized modeling techniques that are used to simulate the boom lenticular joints. System level models are exercised to understand the boom deployment dynamics and spacecraft level implications. Discussion includes a comparison of ADAMS simulation results to measured flight data taken during the three boom deployments. Important parameters that govern lenticular joint behavior are outlined and a short summary of lessons learned and recommendations is included to better understand future applications of this technology.

Nomenclature

α	=	mass proportional damping coefficient
β	=	stiffness proportional damping coefficient
$[C]$	=	Rayleigh damping matrix
$\{f_d\}$	=	damping force vector
$[K]$	=	structural stiffness matrix
$[M]$	=	structural mass matrix
$\{V\}$	=	component velocity vector
ζ_i	=	i^{th} modal damping
ω_i	=	i^{th} modal frequency
$\{Y\}$	=	component displacement vector

I. Introduction

THE Mars Advanced Radar for Subsurface and Ionosphere Sounding (MARSIS) antenna is part of an instrument payload onboard the European Space Agency's (ESA) Mars Express (MEX) spacecraft which launched on June 2, 2003 and entered Mars orbit on December 25, 2003. MARSIS is a long wavelength radar sounder that will be used to perform measurements on the Martian ionosphere and to search for evidence of subsurface water. It is designed to operate at altitudes up to 800 km above the Martian surface for subsurface sounding, up to 1200 km for ionospheric sounding, and is capable of making measurements in 1 MHz wide bands centered at 1.8, 3.0, 4.0, and 5.0 MHz. This flexible design allows MARSIS to search for evidence of water as deep as 5 km below the surface.

The antenna for the MARSIS experiment was developed and built by NGST Astro Aerospace. The antenna is made of three Foldable Flattenable Tubes (FFT)™. A full description of the design is presented in Ref. 1. The FFT is an ultra-lightweight deployable structure that is designed purely for use in a space environment. As such, any significant friction, gravity, or air drag, combined with its large dimensions, renders terrestrial based testing of the

* Chief Analyst, Engineering, 6384 Via Real, Member AIAA.
† Senior Engineer, Spacecraft Structures and Dynamics Group, 4800 Oak Grove Dr., MS: 157-500, Member AIAA.

Copyright © 2006 by the American Institute of Aeronautics and Astronautics, Inc. All rights reserved.

FFT intractable. Therefore, the verification process for the FFT deployment relied solely on component level testing and analytical simulations performed using ADAMS software.

The original deployment simulation of the MARSIS antenna, done in 2000, underestimated its dynamics due to misleading documentation of damping in ADAMS and an overestimate of the hinge strength. The typical damping implementation in software used for dynamic analysis, such as ADAMS or DADS, does not work properly for time variant structures such as the FFT. The correct application of damping for time variant structures should be the implementation of structural or hysteretic damping. In early 2004, during the design and analysis of a much shorter FFT for the SHARAD (SHAllow RADar) antenna, it was discovered that the term 'structural damping' in the ADAMS manual is used incorrectly to describe a 'Rayleigh damping' implementation. As a result of this error, the ADAMS model of the MARSIS antenna had unrealistic modal damping that varied from 188% to 1% during the deployment instead of a constant 1% as intended. This artificially high damping resulted in benign behavior during the original deployment analysis which did not show any significant dynamics. However, after correcting for the application of damping in 2004, the new deployment analysis showed significant dynamics in which the FFT hinges would undergo multiple buckling events during the deployment. This resulted in a highly dynamic and chaotic behavior. This information was immediately communicated to both JPL and ESA.

The deployment of MARSIS, which was initially scheduled for April 20, 2004, was delayed after the discovery that original analysis had underestimated the deployment dynamics. Over the course of the following year an intense analysis and testing effort was undertaken that focused on more accurately quantifying the deployment, validating the ADAMS model, and assessing any risk to the health of the Mars Express spacecraft. Component testing went beyond the original tests done in order to characterize the post buckling behavior of the hinges and their residual strength capability after multiple buckling events. This was necessary since repeated buckling was anticipated based on the increased dynamics in the updated model. The FFT is not designed to take any significant buckling during the deployment and, if the excess dynamics were known at that time, the MARSIS design would have been modified to reduce its stowed energy. Component test results were incorporated into an updated ADAMS model of the deployment which included an automated damping algorithm to account for the discontinuous boom lengths encountered during the deployment. This model was then exercised in a Monte Carlo study in order to determine the probability of a successful or dangerous deployment outcome.

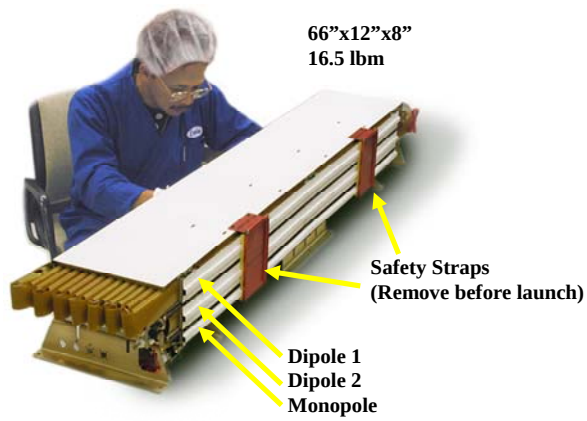

Figure 1. The stowed MARSIS antenna FFT booms and cradle prior to launch.

MARSIS employs a total of three FFT booms with two that form a 40 m dipole and the third acting as a 7 m monopole antenna. The booms have periodic slotted hinge sections where some material is removed which then allows the Kevlar and fiberglass composite tubes to be folded elastically without permanent deformation. The folded booms are then compressed accordion style into a cradle for launch and the journey to Mars as shown in Fig. 1. Each boom is thus a single piece structure in its deployed state with all joints fastened and bonded prior to launch. The deployed dipole and monopole antenna configuration is illustrated along with the Mars Express spacecraft in Fig. 2. The actual antenna is a pair of 22 gage wires that run the length of the interior in all three booms.

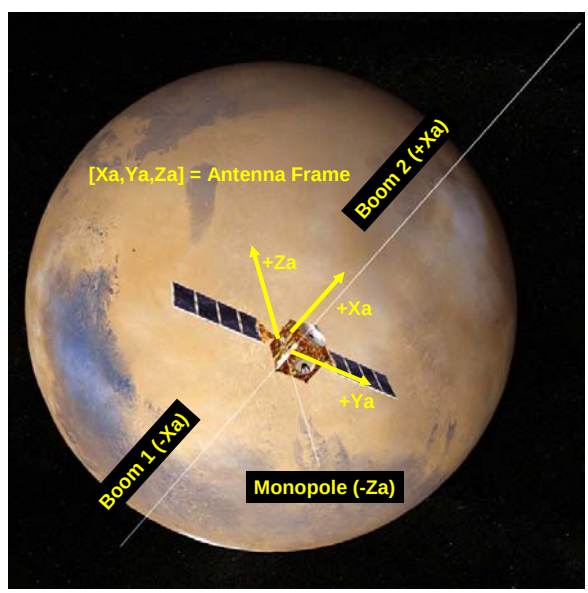

Figure 2. The three deployed MARSIS booms and reference antenna coordinate system.

While the operation of a single lenticular (carpenter tape) hinge is straightforward in a shirt sleeve environment, the simultaneous deployment of

multiple hinges in a space environment has proven to be a challenging problem. Environmental effects, combined with uncertainty in the dynamics, make it impossible to deterministically evaluate the flight behavior of the deployment. The MARSIS mechanical team was faced with the daunting task of quantifying the potential boom dynamic behavior and determining the corresponding risk to the spacecraft given only limited knowledge of the boom properties (post buckling) on station. The pre and post-deployment analysis proved formidable and brought to light the uncertain nature inherent to the deployment of serially linked lenticular hinges. As mentioned previously, one of the key issues with a large deformation deployment such as MARSIS is that friction, gravity, and aerodynamic resistance forces dominate terrestrial testing. The boom is extremely lightweight and its properties are also temperature dependent. As a result of the influence of these forces it is impossible to test the full system behavior prior to flight and we must rely on analysis to predict the deployment dynamics.

II. Analysis Approach and Validation

ADAMS software was utilized as the primary analysis tool and a highly specialized ADAMS model was used to simulate all three of the MARSIS boom deployments. The model was constructed with 13 straight segments connected by spline hinge joints that reproduced the measured hinge torque profile, buckling strengths, and post buckling behavior. Each of the 13 straight segments was composed of two beam elements that employed an automated algorithm to update the damping factor parameter based on the local straight section beam length and the corresponding end conditions. Note, in ADAMS, the term 'structural damping' is used for stiffness proportional Rayleigh damping, which was still used but in a highly modified and discontinuous fashion. Finally, the accordion style stowed state was modeled with gap springs connecting adjacent boom segments in order to capture the stowed compressive energy. The schematic of the dipole boom system is presented in Fig. 3.

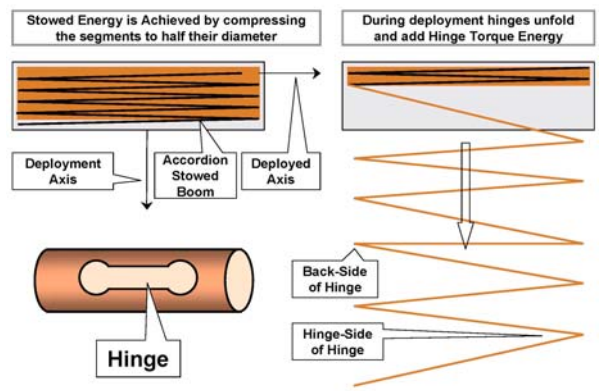

Figure 3. Dipole construction, stowage, and deployment process.

A. Damping Implementation

The damping force $\{f_d\}$ due to Rayleigh or proportional damping $[C]$ is given by[2]:

$$\{f_d\} = [C]\{V\} \tag{1}$$

where $\{V\}$ is the component velocity vector and

$$[C] = \alpha[M] + \beta[K] \tag{2}$$

where $[M]$ is the mass matrix, $[K]$ is the stiffness matrix, and α and β are the mass and stiffness proportional constants. In ADAMS, only the stiffness proportional damping factor β is used and is termed the 'structural damping' factor. The modal damping ζ_i for the ith mode is given by:

$$\zeta_i = 0.5\beta\omega_i \tag{3}$$

where ω_i is the natural frequency of the ith mode.

The use of proportional damping is acceptable for time-invariant structures where the damping factor, β, is selected based on the modal damping of the structure's fundamental mode. When this is done, a higher modal damping will be observed at the higher modes which somewhat represents the behavior of real structures. However, in time-variant structures such as the MARSIS booms, the use of a single Rayleigh damping value is not acceptable since the modal damping for the fundamental mode should always be the same regardless of its natural frequency value.

In the case of the MARSIS antenna, the natural frequency of first two segments at the tip after their connecting hinge becomes fully locked is about 15 Hz; for a modal damping of 1% the damping factor β should be 2E-4. On the other extreme, the natural frequency of the fully deployed antenna is about 0.08 Hz; in this case, the damping factor β should be 0.04 to achieve 1% modal damping. The same damping factor β used for the fully deployed antenna would result in unrealistic modal damping of 188% if applied for the two straight segments.

An automated routine was written and implemented as a user defined beam element in the ADAMS software to mitigate this issue. The routine updates the damping factor β for each individual segment after a hinge changes state (either unlocked to locked or locked to unlocked) and the local straight section (composed of 1 to 13 segments) takes on a different natural frequency. Four different configurations were selected to compute the straight section's fundamental natural frequency: pinned-free for the tip section, pinned-pinned for interior section, and both fixed-pinned and fixed-free for the root section. At each time step the program would examine the current configuration and determine the state of each hinge. Then, using these hinge states, the program would assign an appropriate β for each segment based on the length and boundary conditions of its parent straight section. This approach is somewhat non-conservative since the damping factor β is computed assuming each segment would vibrate at its fundamental mode and during the ADAMS simulation it was observed that some segments did vibrate at higher modes (e.g., immediately after a hinge locks or unlocks).

In separate effort a different approach was used to solve this problem by utilizing a true structural damping model. A version of structural damping was incorporated into ADAMS software and used to validate the first approach. However, the actual time to run a single problem was over 30 hours which made the solution prohibitively slow. The damping force $\{f_d\}$ due to structural or hysteretic damping ε is given by[3]:

$$\{f_d\} = \varepsilon[K]\{|Y|sign(V)\} \tag{4}$$

where {Y} is the component displacement vector and the relation between modal damping ζ and structural damping is given by $\varepsilon = \pi\zeta$.

B. Model Verification

Because a ground based full system deployment test for the MARSIS booms was not possible, relying on analysis was the only way to determine its on-orbit deployment characteristics. Therefore, validation of the ADAMS model was critical in order to substantiate any resulting conclusions. The validation process was accomplished through component static testing combined with simplified dynamic testing. Test results are described in the next section.

In addition, a second model was commissioned using ABAQUS software in order to gain more insight into the hinge behavior both in quasi-static and dynamics environments. The deployment from the stowed configuration of a two segment antenna, connected with a mid hinge, was evaluated in the ABAQUS analysis as shown in Fig. 4. In the quasi-static mode the ABAQUS model deployment was used to characterize the hinge deployment torque, buckling capability, and post buckling behavior. A typical torque profile from this analysis is presented in Fig. 5 and the associated buckling strength is presented in Fig. 6. The predicted hinge stiffness in Figs. 5 and 6 is similar to published analytical and finite element results[4,5] although the primary modeling objective was to explore the buckling mechanisms. In the dynamic mode the stowed constraint was removed suddenly simulating the opening of the cradle door allowing the dynamic deployment of the segments. The purpose of this dynamic analysis was to evaluate the buckling capability of the hinge under dynamic loading. It was concluded that the bucking capability of the hinge is similar for both the static and dynamic environments.

Finally, a third model was also commissioned using DADS software to help verify the ADAMS computational (numerical) routine by creating two similar models in ADAMS and DADS. Note the implementation of damping in DADS (component modal damping) would result in similar erroneous result for time variant structures. Therefore these models were limited in size with most having one or two hinges. The results between ADAMS and DADS were consistent.

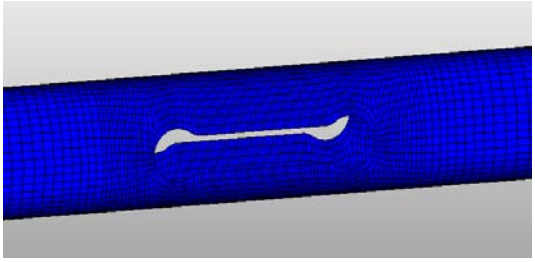

Figure 4a. Undeformed FFT hinge area mesh modeled in ABAQUS.

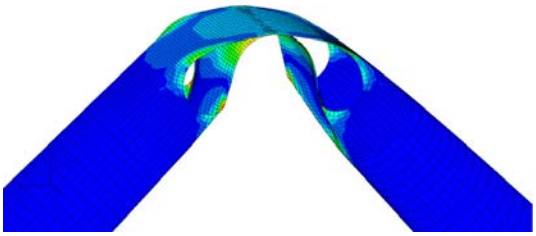

Figure 4b. Hinge area of FFT partially folded with a 45-degree half-angle between the straight segments.

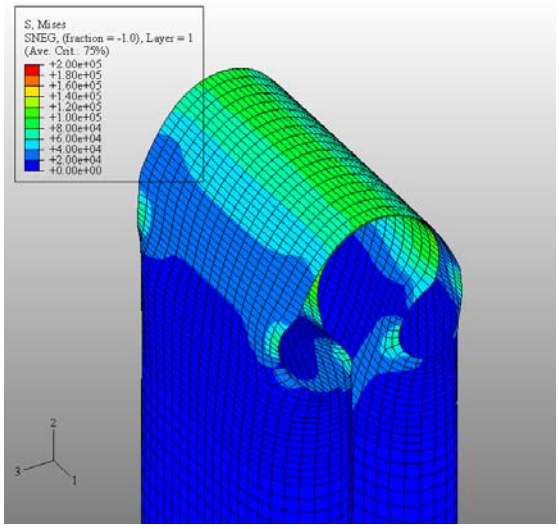

Figure 4c.Hinge area of FFT after folding to a 90° half-angle and compressing the diameter by 50%.

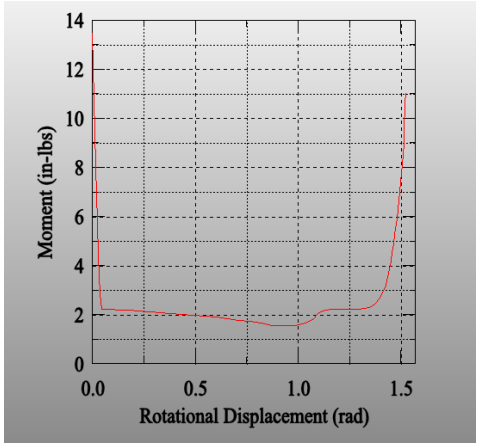

Figure 5. ABAQUS hinge model moment vs. hinge half-angle during quasi-static unfolding.

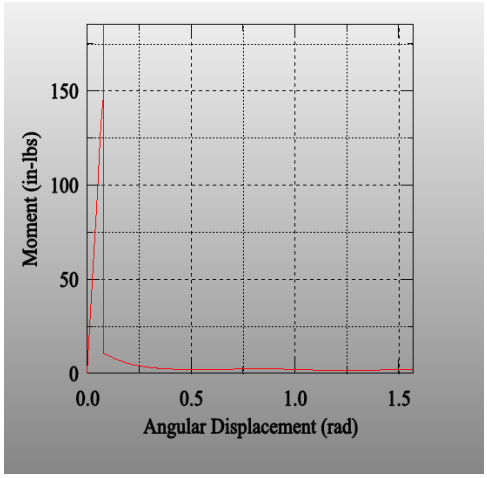

Figure 6a. ABAQUS hinge model buckling moment vs. half-angle displacement.

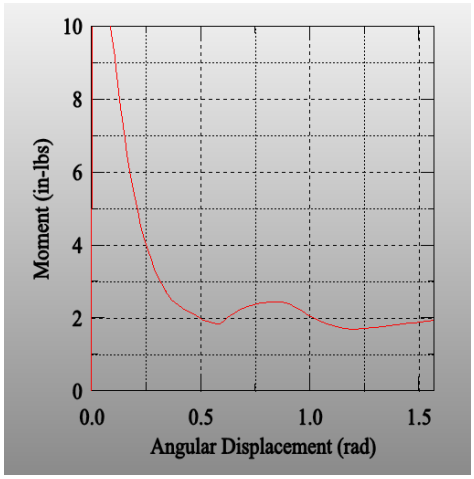

Figure 6b. ABAQUS hinge model post-buckling moment vs. half-angle displacement.

C. Component Testing

Due to the infeasibility of a full system test a computational study was used to determine the critical controlling parameters of the deployment. This resulted in narrowing the planned component testing to three major parameters: the hinge buckling strength, the hinge torque profile, and the stowed compressive energy.

1. Hinge Buckling Strength

The hinge buckling strength was measured using sections of the flight spare booms in a four-point bending fixture. The spare booms were from a qualification unit and were kept in the stowed configuration from the time of launch. Results from this test indicated that the in-situ hinge strength was lower than previous measurements mainly due to thermal environment and aging. Also the hinge buckling could occur both in and adjacent to the hinge section. The mechanism for buckling in the vicinity of the hinge section is illustrated by the ABAQUS results shown in Fig. 7. There was a reduction in hinge buckling strength after a buckling and post buckling cycle due to some fiber failure and localized matrix damage. However, after many buckling cycles, the hinges were still able to deploy and become fully locked with minimal stiffness reduction and their residual strength was adequate for on-orbit operation. A typical buckling and post-buckling behavior of the hinge used in the ADAMS analysis is presented in Fig. 8.

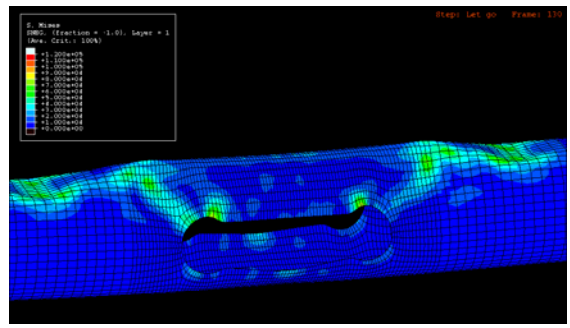

Figure 7. ABAQUS dynamic simulation results showing buckling of the straight tube section at locations outside of the slotted hinge area.

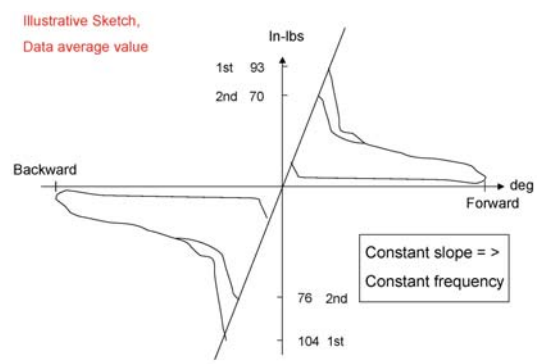

Figure 8. Hinge model for buckling and post-buckling torque used in ADAMS.

2. Hinge Torque

The hinge torque was measured in an environmental chamber at its on-orbit temperature of -70 C to better characterize its contribution to the deployment energy as well as the hysteresis energy dissipation associated with hinge buckling and post-buckling events. The average hinge torque profile used in the ADAMS dynamic simulation is shown in Fig. 10. Note the negative torque region near 40 degrees which represents a secondary stability point and is associated with "freezing" or "stalling" of the hinge.

3. Stowed Energy

In a third series of tests the stowed energy due to the compression of the tube diameter in the cradle was measured in a vacuum chamber at -70 C and found to be 215 in-lbs for the two dipole booms and 38 in-lbs for the monopole boom.

4. Natural Frequency and Modal Damping

A 10 m segment of antenna (half of the 20 m flight length) was used to validate the antenna finite element model and determine its modal damping. The antenna segment was tested in a vertical cantilevered configuration by releasing the tip from a deflected position and measuring the decaying tip motion. Determination of modal damping was done by simulating the test configuration in ADAMS which included the effects of gravity and air drag.

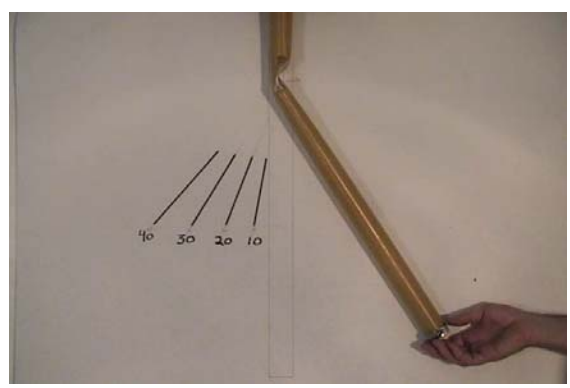

Figure 9. Vertical Pendulum Test to validate the ADAMS hinge model implementation.

Table 1. Comparison of critical ADAMS model parameters.

Critical Parameter List:	Pre-Launch	April & May 04	Current
Modal Damping (%)	~188 *	3.5	3.5
Stowed Energy (in-lb)	350	280	215
Hinge Deploy Energy (in-lb)	~3.0	~3.0	1.5
Hinge Buckling Torque (in-lb)	120/160 **	120	104 & 93
Hinge Post Buckling Hys. (in-lb)	~2.0	~2.0	7.5 & 5.7

* *The original damping parameters were caused by incorrect ADAMS S/W modeling documentation*

** *The hinge buckling used in pre-2000 analysis is 120 in-lbs. After the excess dynamics was discovered one brand new spare sample was tested to 160 in-lbs*

Table 2. Parameters varied in the Monte Carlo analysis.

Variable	Nominal	Range	Distribution	Description
ζ_1	3.5%	2% - 5%	Gaussian	Beam modal damping
SFACTOR	0.6	0.4 - 0.8	Uniform	Hinge spline scaling factor (used to vary the hinge torque profile & energy)
ENERGY	215	205 - 225	Uniform	Stored compressive energy (in-lb)
ABUCKLE	104	78 - 130	Uniform	A-side or back buckling direction hinge strength (in-lb)
BBUCKLE	0.9	0.8 - 1.0	Uniform	B-side or hinge direction strength as a fraction of the A-side strength
PBM1	36.8	18.4 - 55.2	Uniform	Post buckling moment 1 (in-lb)
PBM2	10	5 - 15	Uniform	Post buckling moment 2 scaled using the same fraction of nominal as 1 (in-lb)

5. Vertical Pendulum Test

A single hinge in a vertical pendulum configuration was used to validate the ADAMS hinge model as it buckles dynamically. The test set up is presented in Fig. 9. The hinge properties were determined through static load tests then incorporated into a representative ADAMS model. There was excellent correlation between test and ADAMS simulation (air resistance and gravity was considered in the analysis).

D. Inputs to ADAMS Model

A comparison of the critical properties of the MARSIS antenna based on component testing is presented in Table 1. The antenna properties used in the Monte Carlo simulation are presented in Table 2 and Figs. 10 and 11. The residual buckling capability of each hinge after its first buckling was estimated as 75% of the initial value.

E. Analysis Results

A total of 1,000 cases of the ADAMS model were run in a Monte Carlo study of the deployment dynamics. One of the key results from the Monte Carlo analysis was the discovery that a number of scenarios were possible that could result in the

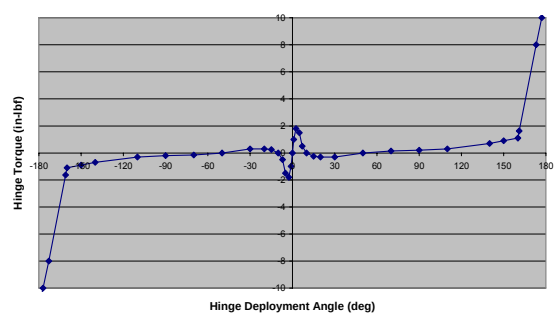

Figure 10. Average hinge deployment torque profile at -70 C.

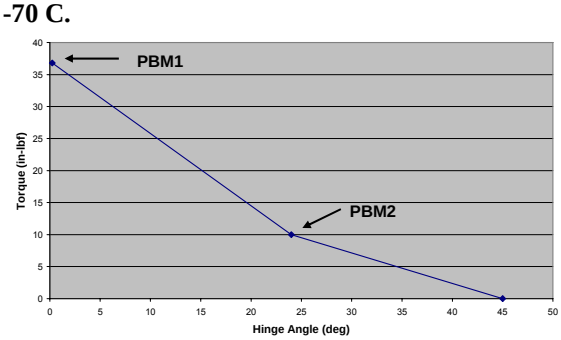

Figure 11. Nominal A-side supplementary post-buckling torque.

boom re-contacting the spacecraft during the deployment. Due to the high stowed compressive energy the dipole boom reaches its full 20 m length in about 2.5 s, after which, it typically experiences a "bullwhip" type behavior and tends to fold back towards the spacecraft in two or more sections. The margin against boom re-contact was quantified based on the closest buckled hinge after the full length of the boom was reached and it was recoiling towards the spacecraft. An illustration showing the erosion of the re-contact margin as the buckled hinge moves closer to the spacecraft is presented in Fig. 12.

Table 3. Summary of Monte Carlo re-contact types and probabilities.

	Contact Cases	Slap Cases	Fold Cases	Cradle Cases
Boom 1	26%	15%	8%	3%
Boom 2	24%	13%	9%	2%

Results from the Monte Carlo study, shown in Fig. 13 and Table 3, indicated that there was a significant probability that the boom could contact the spacecraft or solar arrays during the deployment. The re-contact cases tended to fall into one of three general categories: 1) a "slap" case (usually with a single buckled hinge) where the boom would have a sweeping motion so as to re-contact with the side of the boom, 2) a "poke" or "fold" case

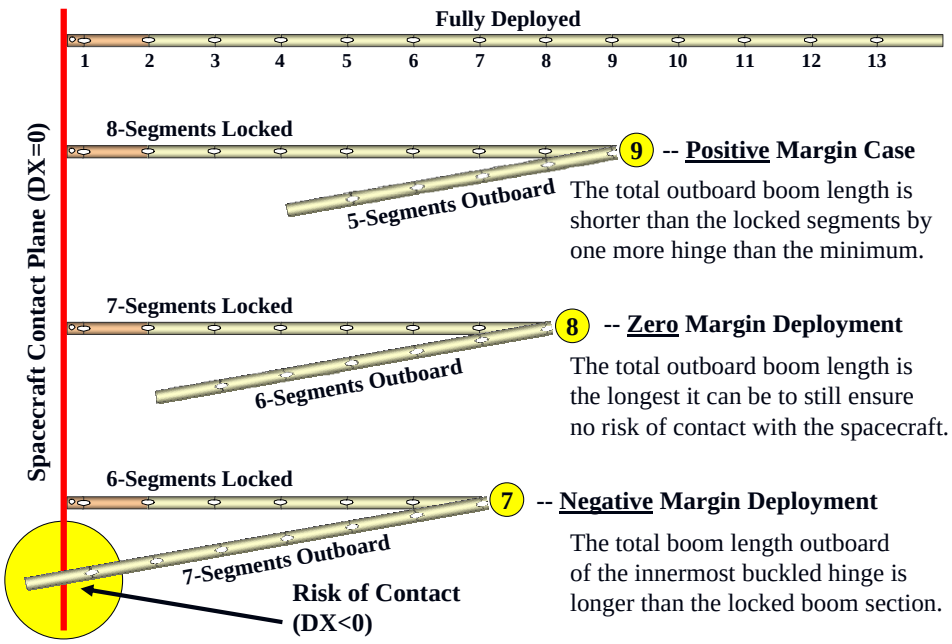

Figure 12. Boom re-contact margin is determined according to the buckled hinge closest to the spacecraft after the initial full extension of the boom (single hinge case shown).

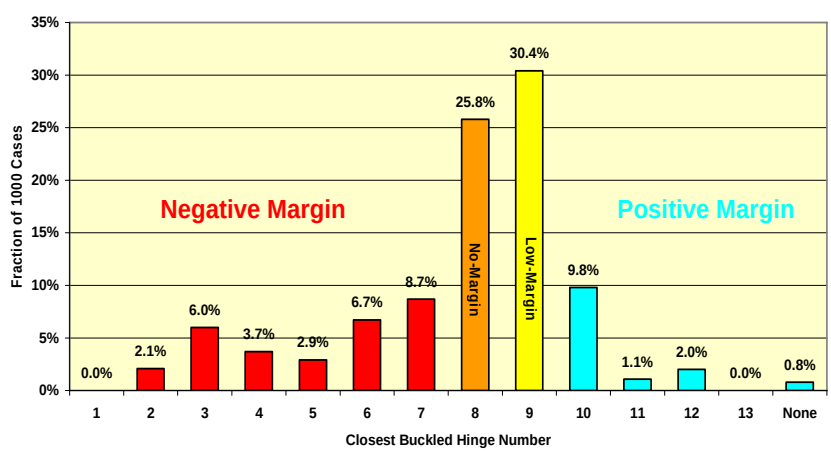

Figure 13. Nominal Monte Carlo closest buckled hinge results at 2.5 seconds for all 1000 cases.

(always with two or more buckled hinges) where the motion of the tip section of the boom was generally aligned with its long axis such that the tip would strike first, and 3) a "cradle" case which involved multiple buckled hinges and the risk that the boom could become entangled itself or on the spacecraft. In order to simplify the onerous task of assessing all 1,000 cases a simple rule was applied that classified any penetration of the plane normal to the initial deployment as having a risk of contacting the spacecraft.

Fig. 14 shows results from the first Monte Carlo run and indicates the total boom kinetic energy (KE), the cumulative number of hinge buckling events, and the point of closest approach for any beam node outboard of the buckled hinge closest to the spacecraft (not counting the root hinge). Note that the buckling events and the point of closest approach are plotted on the right hand axis where the point of closest approach has been multiplied by a factor of 2 to make it more visible. Anytime the point of closest approach line intersects the X-axis then there is zero clearance to the X=0 plane and the case is considered as presenting a risk of contact with the spacecraft. This metric is conservative as it does not include any 3-D motion which would considerably lower the probability. It is also interesting to note the sharp rise in buckling events that leads to a rapid decrease in kinetic energy at about 2.5 s. This is when the boom reaches its initial maximum extension and snaps through its nominal state due to the associated whipping action.

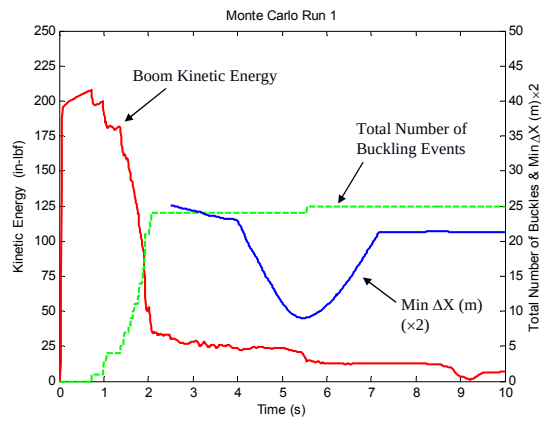

Figure 14. Aggregate Monte Carlo kinetic energy, hinge buckling, and outboard boom clearance results.

A failure modes analysis was done at ESA based on the energies and incidence angles obtained from the Monte Carlo runs. The conclusion of this analysis was that, while significant damage to the spacecraft was possible, the likelihood of it occurring was very low and the decision was made to proceed with the deployment.

III. Flight Deployment

Preparations for the flight deployment proceeded concurrently with the latter stages of the analysis and, once the risks had been vetted, the process necessary to deploy the antennas was engaged.

A. Deployment Dynamics Predictions

With no cameras available the onboard sensing of the MARSIS deployment was limited to 8 Hz sampling of the Mars Express rate gyros. All three of the MARSIS booms deploy primarily in the X-Z plane of Fig. 2 where the hinge axes of rotation are nominally aligned with the Y-axis. Because the solar arrays are also deployed along the Y-axis the I_{yy} term is the minimum spacecraft inertia and is also the axis of principal interest as the largest rates were expected to be in the ω_y measurements. Rates about the X and Z-axes are small and are dominated by the response of the solar arrays during the deployment. A compilation of ω_y results from the first 200 Monte Carlo runs is given in Fig. 15 for cases where the only remaining buckled hinge after the initial deployment was hinge-6 thru hinge-10.

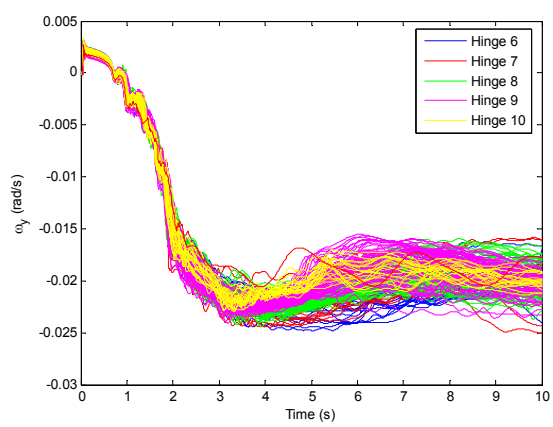

Figure 15. Compilation of ω_y results for all single buckled hinge cases from the first 200 Monte Carlo cases.

B. Flight Deployment Comparison

Dipole boom-1 was deployed on May 4, 2005, after which the spacecraft recovered from its post deployment attitude and was stable. However, telemetry returned from the spacecraft indicated two anomalies in the deployment: first, the deployment dynamics were outside of the Monte Carlo simulations, and second, the spacecraft inertia and

measured natural frequencies both indicated that the boom had not completely locked into place. The latter anomaly is not related to the deployment dynamics modeling and is discussed in the companion paper[6].

The 8 Hz flight data are compared to the average of the single buckled hinge cases in Fig. 16. A separate data set was also constructed that included all the multiple buckled hinge cases for comparison but a search of 1000 Monte Carlo cases did not find a good match. The ω_y rate matched reasonably well over the first 2 s and even the timing of the snatch load agreed quite well with the predicted behavior. However, there were two key features of the flight data in Fig. 16 that appear to have fallen outside of the Monte Carlo analysis: 1) the spacecraft angular rate maintains a nearly constant level over the period from 2 to 7 s, and 2) there is a sharp reversal of the spacecraft rate near 8 s that was not predicted in any of the original 1000 cases. Note that all of the Monte Carlo simulations were carried out for the first 10 s to see if the antenna would impact the spacecraft which was the primary concern. The locking of the root hinge occurs after 10 s and was not observed in any of the cases.

Further details of the complete flight deployment can be seen in the annotated Figs. 17 and 18 showing the spacecraft ω_y through the first 25 and 100 s respectively. In particular, the second snatch loading is immediately followed by what appears to be a "rattling" of the boom which is likely accentuated by the lock-out of the root hinge and a portion of the inboard boom resulting in a mechanical advantage for the loose outboard segments. These characteristics were duplicated in a separate ADAMS model that was modified in an attempt to reproduce this behavior. The

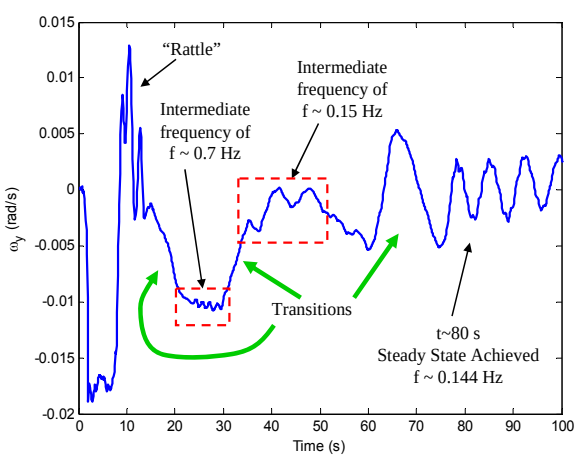

Figure 18. During the subsequent time several intermediate frequencies are observed that likely indicate partially locked boom segments. There were at least 4 individual hinge locking or buckling events following the initial deployment phase (including hinge-10).

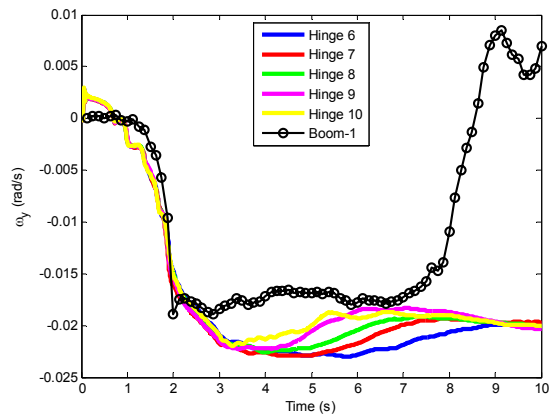

Figure 16. Comparison of flight measured ω_y with average single buckled hinge Monte Carlo results from the first 200 cases.

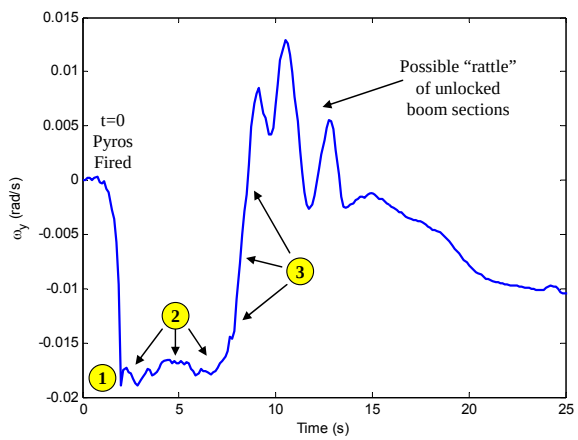

Figure 17. Flight measured ω_y events: 1) initial snatch torque at ~2 s, 2) nearly constant spacecraft rate over ~2 to 7 s suggests that the boom may have multiple buckled hinges with the boom cg following a linear path, 3) indications of possible locking of the root hinge at ~7 s.

ADAMS simulation is presented in Fig. 19 with a comparison of ω_y results to the flight data in Fig. 20. For this run the model was modified to include 0.8% modal damping and increased strength in hinges 1 and 2. Originally hinges 1 and 2 were assigned the same buckling strength as the outer hinges in order to conservatively assess the risk of spacecraft contact. The 0.8% modal damping was determined from the flight data. The explanation for discrepancy between the ground test data (3.5%) and flight data is attributed mainly to the cold temperature. The ground test was performed at room temperature while the flight data were taken at average temperature of -70 C. Test results indicated that the structural or hysteretic damping of the composite material was not temperature dependent. However, there are multiple

bonded splices in the FFT that connect individual boom segments together. The adhesive used to bond the MARSIS tube assemblies was RTV silicone and it is a major contributor to the overall damping. Since the RTV glass transition temperature (Tg) is about -115 C, one could conclude that there would be a significant reduction in damping at cold temperatures.

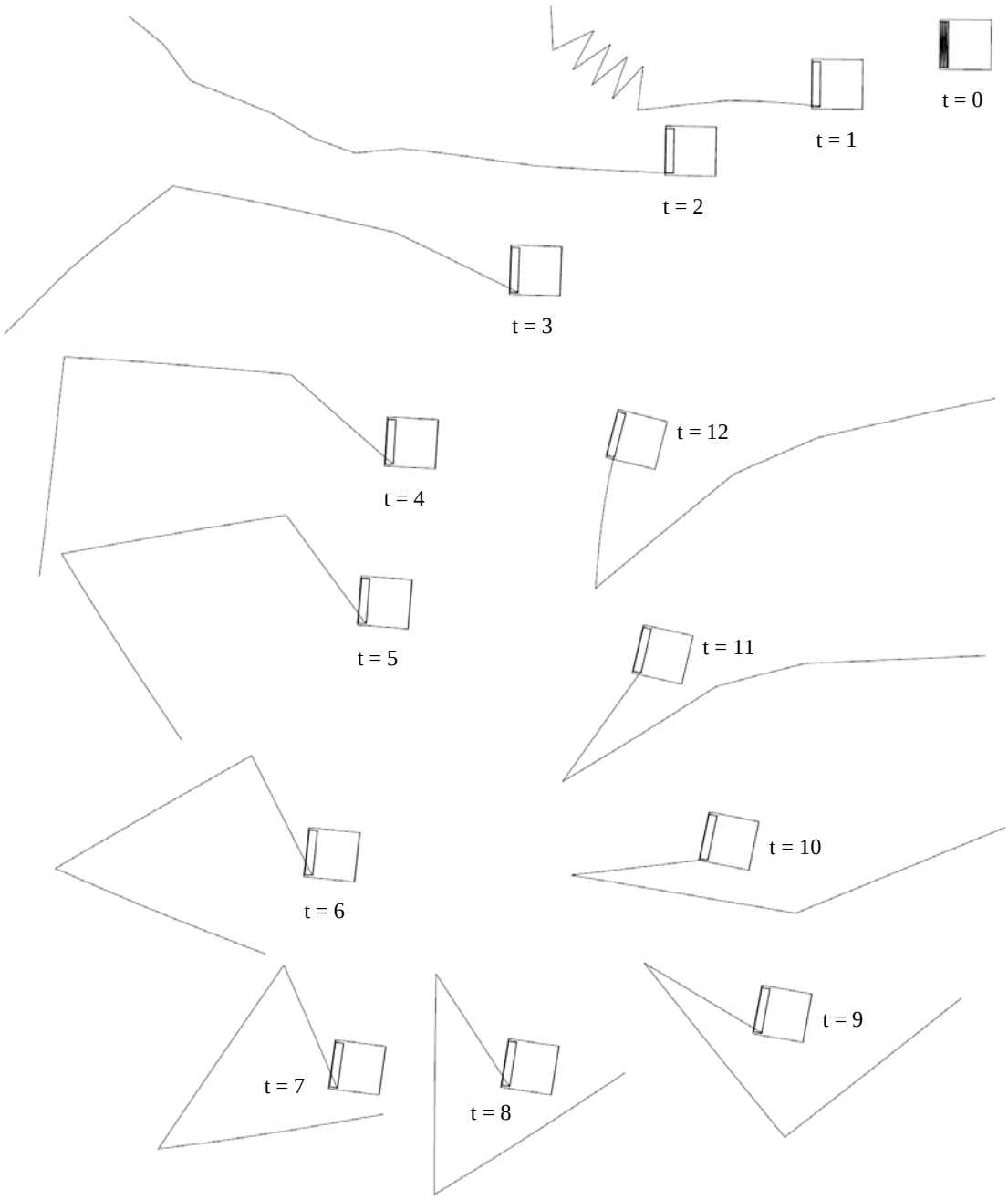

Figure 19. Time sequence illustrating the boom geometries at 1-s intervals for the high hinge-1 and 2 increased strength run with ζ = 0.008. Note that the locking of the root hinge causes a bending moment in the root segments at t = 12 s indicating a strong torque in the opposite direction of the initial boom snatch torque. This sharp reversal of torque was also observed in the boom-1 flight data.

Fig. 18 shows several transitions as the boom slowly reaches varying degrees of deployment until, at approximately 80 s, steady state dynamics are achieved. However, while the steady-state dynamics in Fig. 18 were initially encouraging, the most strongly excited frequency later measured from the flexible modes tests was found to be 0.146 Hz which was well above the predicted value of ~0.1 Hz. In fact, there were three measured frequencies at 0.043 Hz, and 0.146 Hz about the Y-axis and 0.076 Hz about the Z-axes rather than the two expected frequencies at ~0.1 Hz about the Y and Z-axes. This indicated that dipole boom-1 did not achieve a full deployment and the resolution of this incomplete deployment which led to successful deployment is discussed separately in the companion paper[6]. The main problem was that hinge-10 was not fully deployed (~40° short) due to its on-orbit cold temperature (-140 C). Note that hinge characterization was done at -70 C and since the main concern was the high stowed energy the colder deployment was viewed as beneficial in order to reduce the deployment dynamics. Dipole boom-2 was later deployed successfully without any anomalies as was the monopole. The on-orbit telemetry is not adequate to detect the dynamics and consequently the full deployment of ultra lightweight Monopole (0.31 lb) boom.

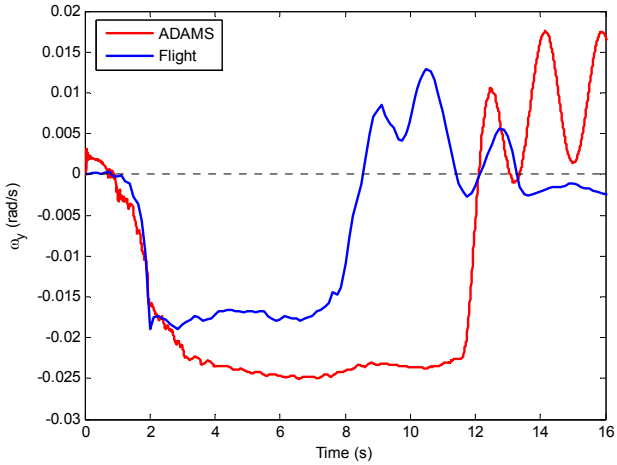

Figure 20. Comparison of flight measured angular rates with the ADAMS results illustrated in Fig. 19. Note the key salient features common to both curves which include a rapid increase in rate near 2 s followed by a period of nearly constant angular rate and then a sharp reversal in the direction of rotation.

IV. Concluding Remarks

First and foremost, the authors strongly recommend that the reader not take lenticular (carpenter tape) structures for granted. The mechanisms and sensitivities of these joints are complex and the use of multiple hinges greatly amplifies the modeling challenges. Material selection and construction can have subtle effects on the hinge behavior which, depending on the materials chosen, can also be strongly dependent on the in-situ temperature. Ideally the hinges should have a positive torque margin throughout their range of motion. These hinge characteristics should be tested to verify their torque characteristics. The tests should closely approximate flight conditions especially temperature, aging, and thermal cycling effects such as from aerobraking, whenever possible.

The total stowed energy should be optimized (neither to high nor low) to control the dynamics in the deployment. The tube compression energy should be low enough to prevent the back-buckling phenomenon but, simultaneously, the hinge energy needs to be high enough to produce positive torque throughout the hinge range of motion. These types of lenticular booms are extremely lightweight and, once in their proper deployed state, are very easily modeled and accounted for on the spacecraft. Unfortunately, it is not possible to perform a meaningful full system test on the ground so an accurate component model of the boom is extremely important.

Acknowledgments

The authors would like to acknowledge the hard work and thorough analysis of the ESA and EADS Astrium engineering and flight team as well as the important contributions of the analysis groups at Boeing Phantom Works for the DADS analysis and at ABAQUS West for the ABAQUS hinge analysis. In particular, the authors would like to thank Lou Adams and Olav Hallberg for their diligent work on the ADAMS simulation. The odyssey of MARSIS was indeed a job well done. The research described in this paper was carried out at NGST Astro Aerospace (Contract No. 1263269) and at the Jet Propulsion Laboratory, California Institute of Technology, under a contract with the National Aeronautics and Space Administration.

References

[1]Marks, G.W., Reilly, M.T., and Huff, R.L., "The Lightweight Deployable Antenna for the MARSIS Experiment on the Mars Express Spacecraft," 36th Aerospace Mechanisms Symposium, Glenn Research Center, May 14-17, 2002.

[2]Thomson, W.T., *The Theory of Vibration with Applications*, 2nd Ed., Prentice-Hall, New Jersey, 1981.

[3]Clough, R.W. and Penzien, J., *Dynamics of Structures*, McGraw-Hill, New York, 1975.

[4]Silver, M. J., Hinkle, J. D., and Peterson, L. D., "Modeling of Snap-Back Bending Response of Doubly Slit Cylindrical Shells," Proceedings of the 45th AIAA Structures, Structural Dynamics and Materials Conference, Palm Springs, CA, April 2004.

[5]Seffen, K.A. and Pellegrino, S., "Deployment Dynamics of Tape Springs," Proceedings of the Royal Society of London Series A, Vol. 455, 1999, pp. 1003-1048.

[6]Adams, D. S., and Mobrem, M., "MARSIS Antenna Flight Deployment Anomaly and Resolution," 47th AIAA Structures, Structural Dynamics, and Materials Conference, May 1-4, 2006, Newport, Rhode Island, AIAA-2006-1684.